HOKKAIDO UNIVERSITY

Title	Photocatalytic Activity of Radial Rutile Titanium(IV) Oxide Microspheres for Aerobic Oxidation of Organics
Author(s)	Kojima, Ryota; Ohtani, Bunsho; Tada, Hiroaki
Citation	ChemPhysChem, 23(3), e202100793 https://doi.org/10.1002/cphc.202100793
Issue Date	2022-02-04
Doc URL	https://hdl.handle.net/2115/87959
Rights	This is the peer reviewed version of the following article: R. Kojima, B. Ohtani, H. Tada, ChemPhysChem 2022, 23, e202100793., which has been published in final form at https://doi.org/10.1002/cphc.202100793. This article may be used for non-commercial purposes in accordance with Wiley Terms and Conditions for Use of Self-Archived Versions. This article may not be enhanced, enriched or otherwise transformed into a derivative work, without express permission from Wiley or by statutory rights under applicable legislation. Copyright notices must not be removed, obscured or modified. The article must be linked to Wiley's version of record on Wiley Online Library and any embedding, framing or otherwise making available the article or pages thereof by third parties from platforms, services and websites other than Wiley Online Library must be prohibited.
Type	journal article
File Information	Accepted article.pdf

Hokkaido University Collection of Scholarly and Academic Papers : HUSCAP

A manuscript for Research Article of *ChemPhysChem*

Photocatalytic Activity of Radial Rutile Titanium(IV) Oxide Microspheres for Aerobic Oxidation of Organics

Ryota Kojima,[a] Bunsho Ohtani,* [b] Hiroaki Tada*[a]

[a] Graduate School of Science and Engineering, Kindai University, 3-4-1, Kowakae, Higashi-Osaka, Osaka 577-8502, Japan. [b] Graduate School of Environmental Science, Hokkaido University, Sapporo, Hokkaido 060-0810, Japan, and Institute for Catalysis, Hokkaido University, Sapporo, Hokkaido 001-0021, Japan.

Radial rutile TiO_2 nanorod homomesocrystals (TiO_2-NR HOMCs) or the so-called "sea urchin-like TiO_2 microspheres" were synthesized by a hydrothermal method. TiO_2-NR HOMCs show photocatalytic activities for aerobic oxidative degradation of 2-naphthol under irradiation of UV- and visible light. Further, extremely small iron oxide clusters were formed on the surface of TiO_2-NR HOMCs (FeO_x/TiO_2-NR HOMCs) by the chemisorption-calcination technique to reduce the band gap. The FeO_x-surface modification gives rise to drastic enhancement of the UV- and visible-light activities. Reversed double-beam photoacoustic spectroscopy measurements were performed for TiO_2-NR HOMCs and FeO_x/TiO_2-NR HOMCs to obtain the ERDT (energy-resolved distribution of electron traps)/CBB (conduction-band bottom) patterns. The ERDT/CBB pattern of TiO_2-NR HOMCs consists of two components derived from rutile (C1) and amorphous TiO_2 (C2). In the pattern, the surface electron traps in C2 exist near the CBB to be removed by the FeO_x-surface modification. By taking this finding into consideration, the striking surface modification effect was ascribable to the electrocatalytic activity (or the action as an electron reservoir) of the FeO_x clusters for multiple ORR, the suppression of recombination, and the increase in the visible-light harvesting efficiency.

1. Introduction

The photocatalytic activity of TiO_2 depends on various properties of primary particles such as crystal form, crystallinity, and size.[1] Also, the assembled structure of TiO_2 particles or the mesocrystal structure can have a great impact upon the photocatalytic activity.[2,3] Among the mesocrystals, radial TiO_2 homomesocrystals consisting of rutile TiO_2 nanorods (TiO_2-NR HOMCs) have recently attracted much attention as a promising photocatalyst material due to the unique nano/micro-sized features including high light-harvesting ability by multiple light scattering, large surface area, and easy separation from the reacted solution.[4,5] Nevertheless, the photocatalytic activity remains low probably because of the poor ability of rutile TiO_2 for oxygen reduction reaction (ORR).[6-8] The deep understanding of the photocatalysis of TiO_2-NR HOMCs for the oxidation of organics is crucial for obtaining the guideline for the enhancement of the photocatalytic activity.

Recently, a group of one of the authors (BO) has developed an analytical method, reversed double-beam photoacoustic spectroscopy (RDB-PAS)[9,10] enabling acquisition of ERDT (energy-resolved distribution of electron traps)/CBB (conduction-band bottom) patterns for semiconducting solid materials such as metal oxides, including titania, and carbon nitride.[11,12] It has been confirmed that ERDT/CBB patterns can be used as a fingerprint of samples for identification of solid inorganic compounds,[13] since an ERDT pattern, CBB and total density of electron trap reflect surface structure, bulk structure and surface (or bulk) size, respectively, to characterize totally solid structures. In this study, ERDT/CBB patterns of samples are used to clarify their structural properties and mechanism of their photocatalyzed ORR.

Here we discuss the photocatalysis of TiO_2-NR HOMCs, and the effect of the surface modification by extremely small iron oxide clusters (FeO_x/TiO_2-NR HOMCs) on the photocatalytic activity for the aerobic oxidation of organics on the basis of their ERDT/CBB patterns.

2. Results and Discussion

2.1. Unmodified TiO_2-NR HOMCs

[*] R. Kojima, Prof. Dr. H. Tada*
Graduate School of Science and Engineering, Kindai University, 3-4-1, Kowakae, Higashi-Osaka, Osaka 577-8502, Japan.
E-mail: h-tada@apch.kindai.ac.jp.
B. Ohtani*
Graduate School of Environmental Science, Hokkaido University, Sapporo, Hokkaido 060-0810, Japan, and Institute for Catalysis, Hokkaido University, Sapporo, Hokkaido 001-0021, Japan.
E-mail: ohtani@cat.hokudai.ac.jp

Supporting information for this article is available on the WWW under http://dx.doi.org/10.1002/anie.201xxxxxx.((Please delete if not appropriate))

TiO_2-NR HOMCs were synthesized using a hydrothermal method previously reported.[14] Figure 1A shows SEM image of the samples prepared at hydrothermal reaction time (t_{HT}) = 8 h. The sample consists of radial spherical particles with a mean diameter of 3.4 μm. The specific surface area determined to be 15.2 m^2 g^{-1}, which is ~80 times greater than the value for the dense spherical particles with the same diameter. Figure 1B shows the X-ray diffraction (XRD) pattern of TiO_2-NR HOMCs prepared at t_{HT} = 8 h. Diffraction peaks appear at 2θ = 27.40° and 36.06° indexed as the diffraction from the (110) and (101) crystal planes of rutile TiO_2, respectively (ICDD No. 00-021-1276). Figure 1C and D shows transmission electron microscopy (TEM) and high resolution (HR)-TEM images of the same sample. A TiO_2-NR HOMC is comprised of many rutile TiO_2-NRs with a diameter of ~20 nm, growing in the [001] direction. Also, the surface structure appears to be fairly disordered at an atomic level.

Figure 2A shows the absorption spectrum of TiO_2-NR HOMCs. The absorption steeply rises at around 420 nm with

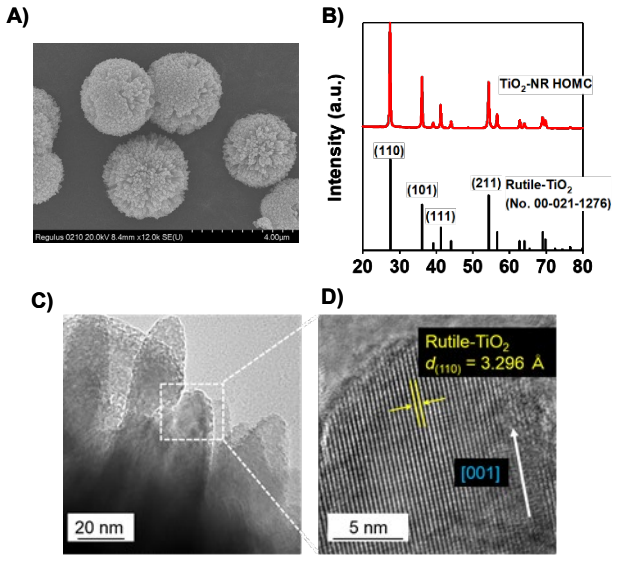

Figure 1. (A) SEM images for the samples synthesized sample prepared at the hydrothermal reaction time (t_{HT}) = 8 h. (B) XRD patterns of the same sample. TEM (C) and HR-TEM (D) images for the same sample.

a weak tail to ~500 nm. From the Tauc plot, the direct band gap[15] was determined to be 3.07 eV. The photocatalytic activity of TiO_2-NR HOMCs (0.1 g) for the degradation of 2-naphthol was assessed in its aerated 10 μM solution (50 mL, solvent = water : acetonitrile = 99 : 1 v/v) under irradiation of UV-light (λ_{ex} = 365 nm) and visible light (λ_{ex} > 400 nm). It should be noted that surface complexes absorbing visible light can be formed at high concentrations of 2-naphthol and acetonitrile in the solvent. Under these conditions, the photocatalytic activity of TiO_2 cannot be strictly assessed because 2-naphthol undergoes degradation via the photosensitized mechanism (Figure S1).[16] We confirmed that the influence of the surface complex can be neglected under the present conditions. In the dark, no change in the concentration of 2-naphthol is observed. The concentration of 2-naphthol gradually decreases with increasing irradiation time under irradiation of UV-light and even visible light.

The ERDT/CBB pattern analysis is adequately applicable to TiO_2-NR HOMCs due to the large specific surface area comparable with that of NPs. In the RDB-PAS measurements, the density of states (DOS) for surface Ti^{3+} levels generated by excitation of TiO_2 are determined under a methanol-saturated nitrogen atmosphere. After the measurement, TiO_2 usually changes from white to blue or gray due to the generation of surface Ti^{3+} ions. When the sample is exposed to air, the color is backed to white. Thus, ERDT/CBB patterns obtained from the RDB-PAS

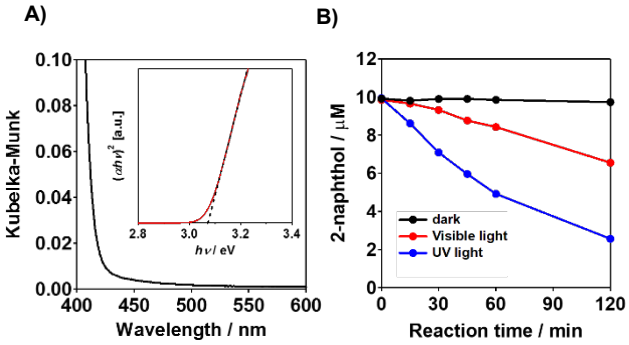

Figure 2. (A) Absorption spectrum of TiO_2-NR HOMCs. (B) Time courses for TiO_2-NR HOMC-photocatalyzed 2-naphthol degradation in the dark, and under UV-light (λ_{ex} = 365 nm, light intensity I = 10 mW cm^{-2}) and visible light (λ_{ex} > 400 nm, $I_{420\sim485\ nm}$ = 10 mW cm^{-2}).

measurements can directly provide information about the surface electronic states taking part in the ORR. Figure 3A shows the PA spectrum of TiO_2-NR HOMCs. From the absorption edge, the band gap was estimated to be 2.95 eV, which is close to the value determined from the absorption spectrum (Figure 2A) and literature value for rutile TiO_2 of 3.0 eV[17] (Figure 2A). As shown in Figure 3B, the RDB-PA spectrum of TiO_2-NR HOMCs steeply at ~440 nm somewhat longer than the absorption edge. Figure 3C shows the resulting ERDT/CBB pattern of TiO_2-NR HOMCs. The pattern consists of at least two components, i.e., one is a narrower component distributing from 2.7 eV to ~3.2 eV with a peak at 3.0 eV (component 1), and the other is much broader

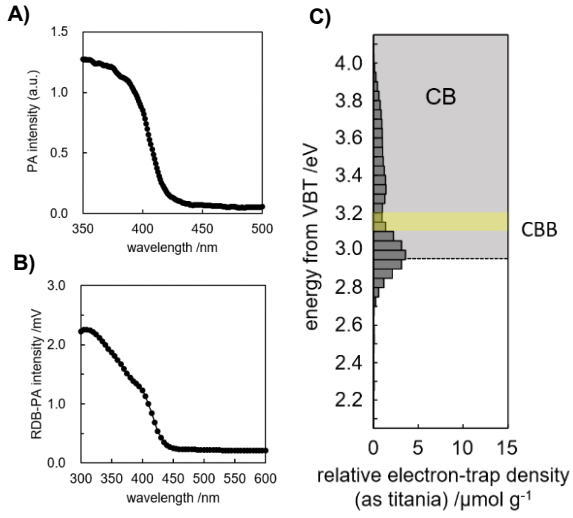

Figure 3. PA spectrum (A), RDB-PAS spectrum (B) and ERDT/CBB pattern (C) of TiO_2-NR HOMCs.

component distributing from ~3.2 eV to 3.9 eV (component 2). The profile of the ERDT/CBB pattern for component 1 is in good agreement with that for pure rutile TiO_2 particles.[18] Also, component 2 suggests the presence of an amorphous layer on the surface of TiO_2-NR HOMCs,[19] which is indicated by the HR-TEM image (Figure 1D). To extract the information about the ORR process from the ERDT/CBB pattern, it is necessary to determine the relative energy of the surface electron traps with respect to the CBB. In the ERDT/CBB pattern of TiO_2, the energy of the surface electron trap was confirmed to be overestimated by 0.1~0.2 eV from the comparison with the value determined by the chemical method using methyl viologen as a probe molecule.[20] This is probably because both of the DOSs of the surface electron traps and the VBT of TiO_2 are small (Figure S2). Thus, the actual CBB level of TiO_2-NR HOMCs is compensated to be 3.1~3.2 eV as shown by the yellow bar in Figure 3C. Importantly, the surface electron trap levels of component 1 and 2 co-exist around CBB.

2.2. FeO_x/TiO_2-NR HOMCs

The surface of TiO_2-NR HOMCs was modified by FeO_x clusters by the chemisorption-calcination technique using $Fe(acac)_3$ with various concentration (C) as a precursor.[21] The amount of Fe in the sample was quantified by inductively coupled plasma spectroscopy to be expressed by the amount per unit surface area (Γ/Fe ions nm^{-2}). The value of Γ increases with an increase in C (mM) according to a Langmuir-type relation $\Gamma^{-1} \approx 0.33C^{-1} + 0.26$ (Figure S3). From the slope and intercept, the saturated Fe-loading amount and the adsorption equilibrium constant of $Fe(acac)_3$ on TiO_2-NR HOMCs were estimated to be 3.85 Fe ions nm^{-2} and 7.9 × 10^2 M^{-1}, respectively. The large adsorption equilibrium constant indicates that $Fe(acac)_3$ is chemisorbed on rutile TiO_2 as well as anatase TiO_2,[22] which is responsible for the formation of extremely small FeO_x clusters on TiO_2-NR HOMCs unobservable even by HR-TEM.[21]

Figures 4A shows the absorption spectra of $FeO_x(\Gamma)/TiO_2$-NR HOMCs. FeO_x-surface modification significantly redshifts the absorption edge from ~420 nm at Γ = 0 to ~480 nm with a tail < ~550 nm at Γ = 3.5. Previous density functional theory simulations for a model of FeO_x/rutile TiO_2 indicated that the apparent decrease in the band gap is caused by the surface sub-band generated above the valence band top (VBT).[23] Figures 4B shows time change of the 2-naphthol concentration in the $FeO_x(\Gamma)/TiO_2$-NR HOMC system under irradiation of UV light (λ_{ex} = 365 nm). The FeO_x-surface modification causes a drastic enhancement in the UV-light activity increasing slightly with an increase in $\Gamma \leq 3.5$. Also, visible-light activity is remarkably enhanced by the FeO_x-surface modification (Figure S4). As shown in Figures 4C and D, the photocatalytic degradation of 2-naphthol apparently follows the first-order rate law. The FeO_x-surface modification increases the rate constants under irradiation of UV-light (k_{UV}) and visible light (k_{Vis}) from 7.2×10^{-3} min^{-1} at Γ = 0 to 7.8×10^{-2} min^{-1} at Γ = 3.5 and 2.1×10^{-3} min^{-1} at Γ = 0 to 2.0×10^{-2} min^{-1} at Γ = 3.5, respectively.

Figure 5 shows the PA and RDB-PA spectra, and ERDT/CBB pattern of $FeO_x(\Gamma = 3.5)/TiO_2$-NR HOMCs. In the PA spectrum (A), a significant redshift in the absorption edge with broad and significant absorption at λ > 500 nm is also observed as a result of the FeO_x-surface modification. From the absorption edge, the band gap was estimated to be 2.6 eV. In the RDB-PA spectrum (B), strong signal is observed in the range of wavelength longer than the absorption edge. A significant change in the ERDT/CBB pattern (C) is induced by the FeO_x-surface modification. Here we assume that component 1 and 2 in the pattern of TiO_2-NR HOMCs undergo perturbation although the possibility of the generation of some new electron traps cannot be excluded. The CBB in $FeO_x(\Gamma = 3.5)/TiO_2$-NR HOMCs can be corrected to be at 3.1~3.2 eV by taking the apparent upward shift in the VBT[23] into consideration as shown by the yellow bar in Figure 5C (Figure S2). In contrast to the TiO_2-NR HOMC system, there is few surface electron traps of component 2near the CBB.

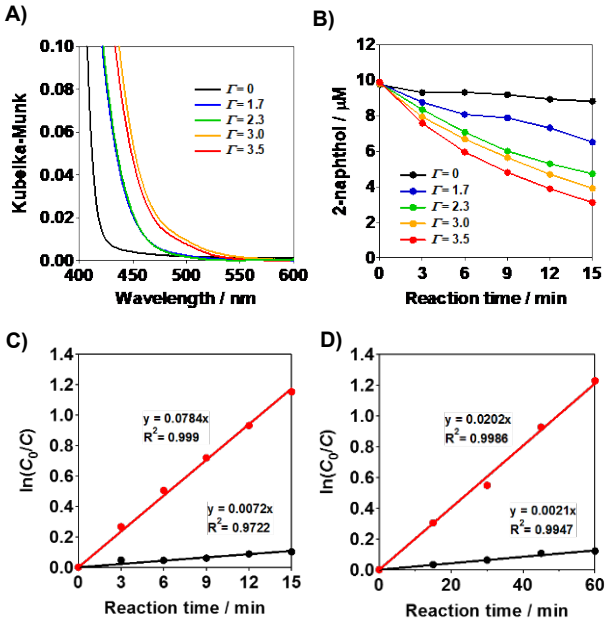

Figure 4. (A) Absorption spectrum of $FeO_x(\Gamma = 3.5)/TiO_2$-NR HOMCs. (B) Time courses for $FeO_x(\Gamma)/TiO_2$-NR HOMC-photocatalyzed 2-naphthol degradation under irradiation of UV light. (C) Plots of $\ln C_0/C$ vs. t_{p}., where C_0 and C are the concentrations of 2-naphthol at t_p = 0 and $t_p = t$, respectively. (D) Plots of $\ln C_0/C$ vs. t_p. in the TiO_2-NR HOMCs (black) and $FeO_x(\Gamma$ = 3.5)/TiO_2-NR HOMCs (red) systems under irradiation of visible light.

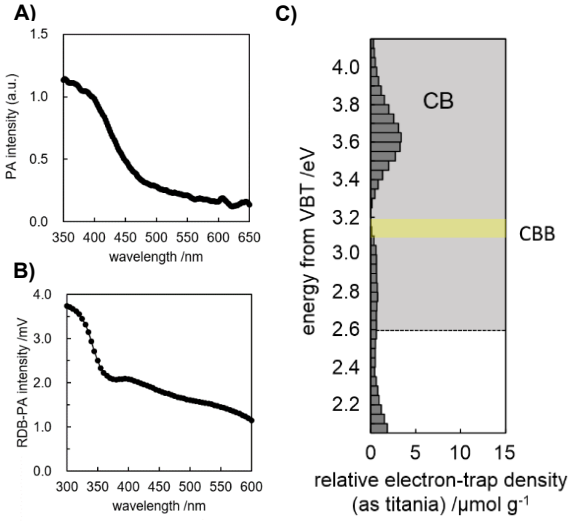

Figure 5. PA spectrum (A), RDB-PAS spectrum (B) and ERDT/CBB pattern (C) of $FeO_x(\Gamma = 3.5)/TiO_2$-NR HOMCs.

The rutile TiO_2-photocatalyzed aerobic oxidation of organics and the drastic enhancement of the activity by the FeO_x-surface modification are discussed on the basis of the energy diagram with the surface electron trap levels. In Scheme 1, the energy level is expressed with respect to the standard hydrogen electrode (SHE) at pH 0. UV-light irradiation of TiO_2-NR HOMCs promotes the electrons in the VB to the CB, and the redox abilities of the resulting electrons and holes are determined by the potentials of the CBB and the VBT, respectively. In the photocatalytic aerobic oxidation of organics, O_2 acts as the acceptor for the electrons excited in the CB, while the holes in the VB directly or indirectly oxidize organics. Rutile TiO_2 is inactive for multiple ORR,[24] and the generation of O_2^- in the rutile TiO_2 photocatalytic reaction was directly confirmed by the chemiluminescence method.[25] However, one-electron ORR ($E^0(O_2/O_2^-)$ = -0.33 V and $E^0(O_2/HO_2)$ = -0.046 V at pH 0)[26] by the CB-electrons with the potential of +0.11 V (vs. SHE at pH 0)[27] is thermodynamically difficult to proceed. Also, the present ERDT/CBB pattern of TiO_2-NR HOMCs indicates that the CB-electrons are trapped by the surface electron traps derived from the amorphous layer (component 2). Amorphous TiO_2 was previously revealed to be photocatalytically inert due to the rapid recombination,[28] and recently, it has also been reported that the presence of an amorphous layer on rutile TiO_2 significantly lowers the photocatalytic activity.[19] Thus, the low photocatalytic activity of TiO_2-NR HOMCs for the oxidation of organics is ascribable to the difficulty of one-electron ORR and the facilitated recombination in the surface amorphous layer. On the other hand, the FeO_x-surface modification imparts the electrocataltyic activity for multiple electron-ORR,[29] whose potential is much more positive ($E^0(O_2/H_2O_2)$ = +0.695 V, $E^0(O_2/H_2O)$ = +1.229 V).[26] In this case, there is a possibility

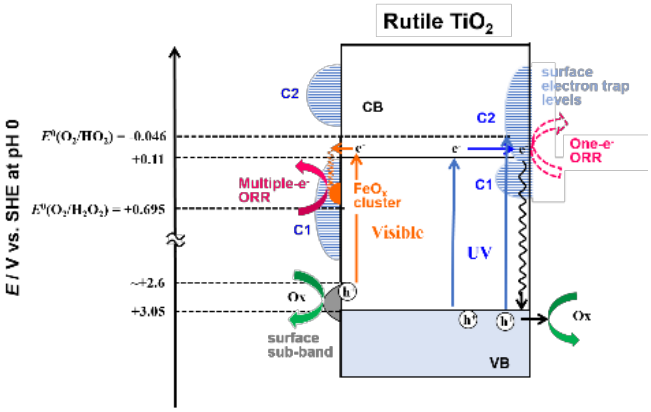

Scheme 1. A proposed mechanism of aerobic oxidation of organics by rutile TiO_2 and FeO_x cluster-surface modified rutile TiO_2.

that the FeO_x clusters act as an electron reservoir. Also, in the ERDT/CBB pattern of FeO_x(Γ = 3.5)/TiO_2-NR HOMCs, the surface electron traps of component 2 near the CBB disappear. Further, the visible light absorption intensifies with the FeO_x-surface modification due to the generation of the surface sub-band above the VBT.[23] Thus, the striking UV-light activity is ascribable to the electrocatalytic activity or the role as an electron reservoir of the FeO_x clusters for multiple-electron ORR and the suppression of the recombination through the surface electron trap levels in the amorphous layer. The same effects of the FeO_x clusters can also be obtained under visible-light irradiation, and additionally, visible-light absorption is enhanced due to the electronic transition from the surface sub-band to the CB of FeO_x /TiO_2-NR HOMCs. Consequently, high activation of the TiO_2-NR HOMC photocatalyst for the oxidation of organics can be achieved under irradiation of UV- and visible light.

3. Conclusions

Radial TiO_2 nanorod homomesocrystals (TiO_2-NR HOMCs) or the so-called "sea urchin-like TiO_2 microspheres" were synthesized, and the surface was modified by extremely small iron oxide clusters (FeO_x/TiO_2-NR HOMCs). The FeO_x-surface modification induces the UV- and visible-light activities for aerobic oxidative degradation of 2-naphthol by approximately one-order of magnitude. The ERDT (energy-resolved distribution of electron traps)/CBB (conduction-band bottom) patterns indicate that the surface amorphous layer-derived electron traps near the CBB in the TiO_2-NR HOMC system are removed by the surface modification with the FeO_x clusters. Consequently, the remarkable surface modification effect can stem from the electrocatalytic activity or the action as an electron reservoir of the FeO_x clusters for multiple ORR, the restriction of recombination, and the enhancement of the visible-light harvesting efficiency. This study has demonstrated that the ERDT/CBB pattern analysis can provide useful information about not only the surface/bulk properties of TiO_2-based photocatalysts but also the mechanism of the photocatalysis.

Experimental Section

Catalyst preparation. According to the method reported in the preceding paper,[14] TiO_2-NR HOMCs were hydrothermally synthesized. Oleic acid (20 mL, Kishida Chemical), 35% hydrochloric acid (2 mL, Wako), and tetrabutyl orthotitanate (4 mL, > 97.0%, Kanto Chemical) was poured into a container made by Teflon (50 mL, HUT-50, SAN-AI Kagaku). The solution was stirred for 15 min at room temperature, and then ultrasonic irradiation was carried out. The Teflon-container was tightly sealed in a stainless-steel cylynder (HUS-50, SAN-AI Kagaku), and the cylinder was heated at 453 K for 8 h in an oven. After the hydrothermal reaction, solid products were obtained from the solution by centrifugal separation. Then, they were purified by repetitive water washing and sentrifugation followed by vacuum drying at room temperature. Iron oxide (FeO_x) clusters were formed on TiO_2-NR HOMCs, by the chemisorption-calcination technique.[21] After TiO_2-NR HOMCs (0.5 g) were added to 50 mL of a $Fe(acac)_3$ solution with varying concentration (C) (solvent, ethanol : n-hexane = 3: 17 v/v), they were allowed to stand for 24 h at 298 K. The resulting samples were washed repeatedly with the solvent for the physisorbed complexes to be removed and dried, followed by heating in air at 773 K for 1 h.

Catalyst characterization. X-ray diffraction (XRD) measurements were performed with a Rigaku Miniflex II diffractometer with CuKα radiation. TEM images were obtained with a JEOL JEM-2100F instrument in a bright-field diffraction contrast mode at an applied voltage of 200 kV. The specific surface area was determined by nitrogen adsorption-desorption isotherms at 77 K with a micromeritics automatic surface area and porosimetry analyzer (TriStar 3000, Shimadzu). Prior to the nitrogen adsorption, all samples were degassed at 423 K for 1 h under vacuum.

Photocatalytic reactions. In the decompositions of 2-naphthol, the reaction cells were irradiated by a Xe lamp (Wacom XRD-501SW) through a high pass filter (L-42, Toshiba) to cut off UV-light ($I_{420\sim485\ nm}$ = 10 mW cm^{-2}) for the visible-light-induced activity test, and a UV-LED lamp (λ_{max} = 365 nm, I = 10 mW cm^{-2}). TiO_2-NR HOMCs (0.1 g) were placed in 50 mL of 10 μM solution of 2-naphthol (solvent, acetonitrile: water = 1 : 99 v/v) in a borosilicate glass container was irradiated. 2 mL of the solution was sampled at a given irradiation time, and the electronic absorption spectra of the reaction solutions were measured using a

spectrometer (Shimadzu, UV-1800) to determine 2-naphhtol concentration from the absorption peak at 223.5 nm.

Reversed double-beam photoacoustic spectroscopy measurements. For the measurement of bandgap to estimate conduction band bottom (CBB) position by photoacoustic spectroscopy (PAS) measurement, a sample holder filled with sample was set in a laboratory-made PAS cell equipped with a MEMS (micro-electro-mechanical system; SparkFun MEMS Microphone Breakout, INMP401 (ADMP401)) microphone module and a glass window attached on the upper side of the PAS cell. The PAS cell was sealed and a light generated from a xenon lamp (Bunkoukeiki BK3) equipped with a grating monochromator and modulated at 270 Hz by a light chopper was irradiated from the upper side of the PAS cell with wavelength scanning from 450 nm to 350 nm with a 1-nm step. Photoacoustic (PA) signal was detected by a digital lock-in amplifier (NF Corporation, LI5645) and recorded with reference to that of graphite. The bandgap of a sample was determined by extrapolating the linear part in the shorter wavelength region.

For the measurement of energy-resolved distribution of electron traps (ERDTs) by RDB-PAS measurement, nitrogen saturated with methanol vapor was flowed through a sample-loaded PAS cell for 30 min (nitrogen flow: 30 mL min^{-1}), then the cell was sealed off with bulbs. The PAS cell was set in an acrylic box and nitrogen was passed through the box to fill with nitrogen. Two light beams combined by a UV quartz combiner light guide (Moritex, MWS5-1000S-UV3) were irradiated from the upper side of the PAS cell. One was a monochromatic continuous light generated from the xenon lamp equipped with a grating monochromator scanned from 650 nm to 350 nm with a 5-nm step to excite electrons from VB to ETs. The other was a 625-nm LED light (Quadica Developments, Luxeon LXHL-ND98) modulated at 35Hz by a digital function generator (NF Corporation, DF1906) to detect PA signal. The PA signal was detected by the digital lock-in amplifier and plotted against photon energy of continuous light. The PA intensity was converted into absolute ET density in the unit of μmol g^{-1} eV^{-1} with factor determined from total ET density measured by photochemical method.[20] The thus-obtained spectrum was differentiated from the lower energy to higher energy to obtain ERDT pattern. To obtain bar-graph type ERDT patterns, the above-mentioned ERDT was replotted with a 0.05-eV pitch.

The authors acknowledge Dr. H. Sugime and Dr. S. Naya for helpful discussion, and A. Akita for experimental support. This work was supported by JST Adaptable and Seamless Technology Transfer Program through Target-driven R&D, JSPS KAKENHI Grant-in-Aid for Scientific Research (C) no. 20K05674, and Nippon Sheet Glass Foundation for Materials Science and Engineering.

Supporting Information:

[1] L. Sang, Y. Zhao, C. Burda, *Chem. Rev.* **2014**, *114*, 9283.
[2] X. Chen, C. Li, M. Grätzel, R. Kostecki, S. S. Mao, *Chem. Soc. Rev.* **2012**, *41*, 7909.
[3] Z. Bian, T. Tachikawa, P. Zhang, M. Fujitsuka, T. Majima, *J. Am. Chem. Soc.* **2014**, *136*, 458.
[4] L. Xiang, X. Zhao, *Nanomaterials* **2017**, *7*, 310.
[5] W.-Q. Wu, Y.-F. Xu, J.-F. Liao, L. Wang, D.-B. Kuang, *Nano Energy* **2019**, *62*, 791.
[6] T. Ohno, K. Sarukawa, M. Matsumura, *J. Phys. Chem. B* **2001**, *105*, 2417.
[7] T. Ohno, K. Tokieda, S. Higashida, M. Matsumura, *Appl. Catal. A* **2003**, *244*, 383.
[8] A. Akita, H. Tada, *Catalysts* **2021**, *11*, 1298.
[9] A. Nitta, M. Takase, M. Takashima, N. Murakami, B. Ohtani, *Chem. Commun.* **2016**, *52*, 12096.
[10] A. Nitta, M. Takashima, N. Murakami, M. Takase, B. Ohtani, *Electrochim. Acta* **2018**, *264*, 83.
[11] C. Chuaicham, S. Karthikeyan, R. R. Pawar, Y. Xiong, I. Dabo, B. Ohtani, Y. Kim, J. T. Song, T. Ishihara, K. Sasaki, *Chem. Commun.* **2020**, *56*, 3793.
[12] C. Chuaicham, R. R. Pawar, S. Karthikeyen, B. Ohtani, K. Sasaki, *J. Colloid Interface Sci.* **2020**, *577*, 397.
[13] A. Nitta, M. Takashima, M. Takase, B. Ohtani, *Catal. Today* **2019**, *321-322*, 2.
[14] D. Sarkar, C. K. Ghosh, S. Mukherjee, K. K. Chattopadhyay, *ACS Appl. Mater. Interfaces* **2013**, 5, 331.
[15] J. Zhang, P. Zhou, J. Liu, J. Yu, *Phys. Chem. Chem. Phys.* **2014**, *16*, 20382.
[16] S. Higashimoto, K. Okada, T. Morisugi, M. Azuma, H. Ohue, T.-H. Kim, M. Matsuoka, M. Anpo, *Top. Catal.* **2010**, *53*, 578.
[17] H. Kisch, *Semiconductor Photocatalysis: Principles and Applications*, Wiley-VCH, Weinheim, **2015**.
[18] Y. Shen, A. Nitta, M. Takashima, B. Ohtani, *Chem. Lett.* **2021**, *50*, 80.
[19] G. Chen, M. Takashima, B. Ohtani, *Chem. Lett.* **2021**, *50*, 644.
[20] S. Ikeda, N. Sugiyama, S.-y. Murakami, H. Kominami, Y. Kera, H. Noguchi, K. Uosaki, T. Torimoto, B. Ohtani, *Phys. Chem. Chem. Phys.* **2003**, *5*, 778.
[21] H. Tada, Q. Jin, H. Nishijima, H. Yamamoto, M. Fujishima, S. Okuoka, T. Hattori, Y. Sumida, H. Kobayashi, *Angew. Chem. Int. Ed.* **2011**, *50*, 3501.
[22] Q. Jin, M. Fujishima, H. Tada, *J. Phys. Chem. C* **2011**, 115, 6478-6483.
[23] M. Nolan, A. Iwaszuk, H. Tada, *Aust. J. Chem.* **2012**, *65*, 624.
[24] H. Tada, S. Naya, *Catalysts* **2021**, *11*, 205.
[25] Y. Kakuma, A. Y. Nosaka, Y. Nosaka, *Phys. Chem. Chem. Phys.* **2015**, *17*, 18691.
[26] *Denki Kagaku Binran*, Jpn. Soc. Electrochem. Ed., Maruzen, Tokyo, **2000**.
[27] G. Cooper, J. A. Turner, A. J. Nozik, *J. Electrochem. Soc.* **1982**, *129*, 1973.
[28] B. Ohtani, Y. Ogawa, S.-i. Nishimoto, *J. Phys. Chem. B* **1997**, *101*, 3746.
[29] H. Yu, H. Irie, Y. Shimodaira, Y. Hosogi, Y. Kuroda, M. Miyauchi, K. Hashimoto, *J. Phys. Chem. C* **2010**, *114*, 16481.

Photocatalysis of Rutile Titanium(IV) Oxide Particles for Aerobic Oxidation of Organics

Ryota Kojima, Bunsho Ohtani,* Hiroaki Tada *

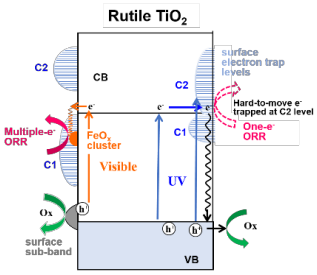

Open the route for ORR: Rutile TiO_2 nanorod mesocrystals show low photocatalytic activities for aerobic oxidation of organics. The surface modification by iron oxide (FeO_x) clusters induces drastic enhancement of the activities. The effect was ascribable to the electrocatalytic activity of the FeO_x clusters for multiple ORR, the suppression of recombination, and the high light harvesting efficiency. The ERDT/CBB pattern analyses indicated that the electron trap levels due to the surface amorphous layer can be removed from the near CBB.